Peer-reviewed version available at Water 2018, 10, 80; doi:10.3390/w10010080

Article

Hydrochemical Characteristics and Multivariate Statistical Analysis of Natural Water System: A Case Study in Kangding County, Southwestern China

Yunhui Zhang [1], Mo Xu [1,*], Xiao Li [1,*], Jihong Qi [1], Qiang Zhang [1], Jian Guo [1], Leilei Yu [1] and Rui Zhao [1]

[1] State Key Laboratory of Geohazard Prevention and Geoenvironment Protection, Chengdu University of Technology, Chengdu, 610059, China; zhangyunhui0710@163.com (Y.Z.); 15317891@qq.com (J.Q.); 435114983@qq.com (Q.Z.); 48280894@qq.com (J.G.); 1292301275@qq.com (L.Y.); 375155702@qq.com (R.Z.)

* Correspondence: XM@cdut.edu.cn (M.X); Tel.: +86-138-081-99827 (M.X); 395605763@qq.com (X.L.); Tel.: +86-138-080-36812 (X.L.);

Abstract: The utilization for water resource has been of great concern to human life. To assess the natural water system in Kangding County, the integrated methods of hydrochemcial analysis, multivariate statistics and geochemical modelling were conducted on surface water, groundwater and thermal water samples. Surface water and groundwater were dominated by Ca-HCO_3 type, while thermal water belonged to Ca-HCO_3 and Na-Cl type. The analyzing results concluded the driving factors that affect hydrochemical components. Following the results of the combined assessments, hydrochemcial process was controlled by the dissolution of carbonate and silicate minerals with slight influence from anthropogenic activity. The mixing model of groundwater and thermal water was calculated using silica-enthalpy method, yielding cold-water fraction of 0.56-0.79 and estimated reservoir temperature of 130-199 °C, respectively. δD and $\delta^{18}O$ isotopes suggested surface water, groundwater and thermal springs were of meteoric origin. Thermal water should have deep circulation through the Xianshuihe fault zone, while groundwater flows through secondary fractures where it recharges with thermal water. Those analytical results were used to construct a hydrological conceptual model, providing a better understanding of the natural water system in Kangding County.

Keywords: Hydrochemcial characteristics; water-rock interaction; multivariate statistical analysis; mixing model; δD and $\delta^{18}O$ isotopes; natural water system; Kangding County.

1. Introduction

Water is an incredibly important resource, and has significant uses in agriculture, industry and domestic use. To better utilize it, a number of researches have been conducted to assess the water quality [1-4]. The water quality is determined by the hydrochemistry affected by different hydrochemical processes. Furthermore, hydrochemical process is determined by natural physical-chemical activities, e.g., ion exchange, mineral dissolution and precipitation, water-rock interaction, and redox transformation [5-7].

Up to date, hydrochemical analysis [8, 9], multivariate statistical analysis [10, 11], and geochemical modelling [12, 13] have been proved to be efficient for constraining the hydrochemical process of natural water system. The ratios of major ions provide critical clues to explain different hydrochemical processes of water resource [14, 15]. Principle component analysis (PCA) is useful to analyze the large hydrochemical dataset, defining the factors controlling hydrochemistry [16, 17]. Geochemical modelling using saturation index can specify the mineral precipitation and dissolution in natural water system [18, 19]. δD and $\delta^{18}O$ isotopes are ideal tracers for the source and pathways of groundwater recharge [20-22].

Southwestern China is well-known for its abundant water resource, including the Dadu River, Jinsha River and Nu River. The Kangding County is located in southwestern China and dominated by the Dadu River. However, previous studies were mainly focused on the genesis of thermal water in Kangding County. Qi et al (2017) achieved a preliminary knowledge of thermal water and discussed the relationship between changing parameters of thermal water and solid tide [23]. Luo et al (2017) compared the thermal springs in northern and southern Kangding County and evaluated the exploring potential [24]. Guo et al (2017) investigated the high-temperature geothermal system using fluid and gas geochemistry [25]. Compared with thermal water, very little knowledge has been achieved on the chemical components of surface water and groundwater and related hydrochemical process. Moreover, the mixing model between groundwater and thermal water is enigmatic, and has yet to be constrained.

In this study, we investigated the occurrence of fractures, interpreted hydrochemical characteristics and conducted δD and $\delta^{18}O$ isotopic analysis for surface water, groundwater and thermal water. Then, we attempted to get deeper knowledge of the hydrochemical process based on correlations of major ions, PCA analysis and geochemical modelling. Furthermore, the mixing ratio between groundwater and thermal water was evaluated by the silica-enthalpy method. The recharge area of surface water, groundwater and thermal water was identified by δD and $\delta^{18}O$ isotopes. Those analytical results would be helpful to build a hydrological conceptual model for natural water system, providing valuable information for better exploiting water resource in Kangding County.

2. Geological setting

Kangding County is situated in the Sichuan Province, southwestern China. Tectonically, it is located in the eastern margin of Tibet Plateau where three regional fault zones (Xianshuihe, Anninghe and Longmenshan fault zones) formed a Y-shape intersection (Figure 1a). The altitude of

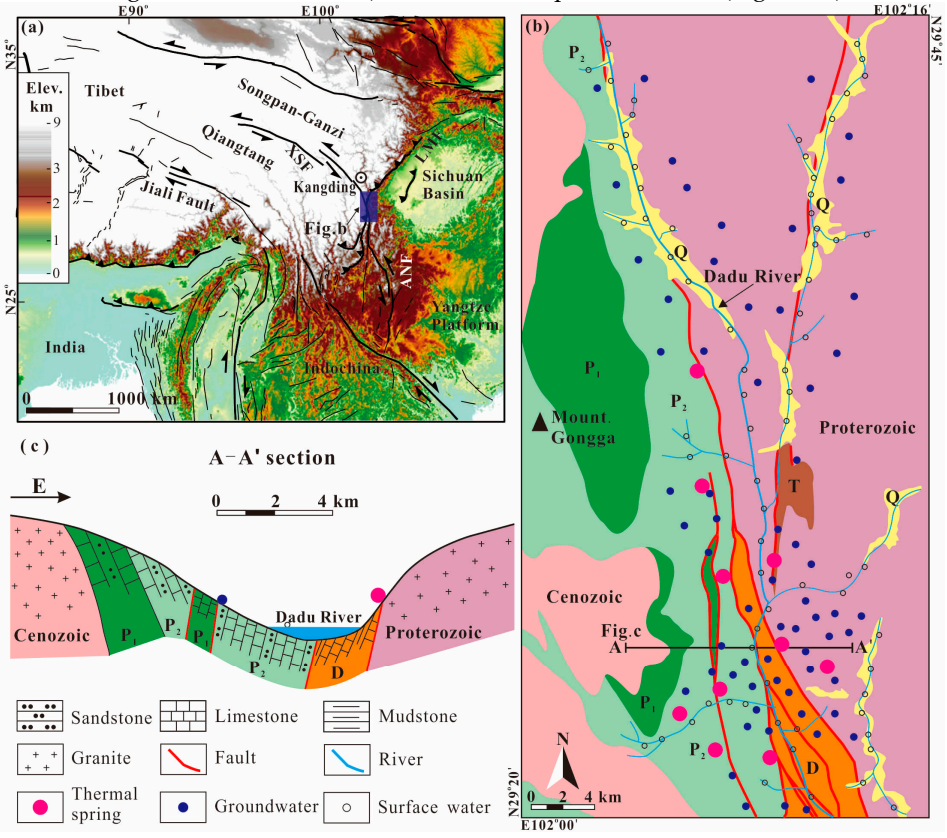

Figure 1. (a) Topography of Southwestern China, (b) geological map and (c) cross section of Kangding County. XSF. Xianshuihe fault, LMF. Longmenshan fault, ANF. Anninghe fault.

Kangding County is generally higher than 1000 m with the highest elevation of 7556m (Mount. Gongga). Due to the high-mountain topography and barren environment, anthropogenic activity is rare here. Based on the local meteorological data, annual precipitation and relative humidity are 500-800 mm and 73%, respectively. Annual temperatures range from -14.1 °C to 29.4 °C (mean = 7.1 °C).

Our study area is located in southern segment of Kangding County. The bedrocks consist of Devonian, Permian, and Triassic sedimentary strata (Figures 1b, 2a). Devonian strata exposed in the south are composed of limestone and mudstone; Permian strata crop in the west and are subdivided into upper and lower Permian strata, consisting of limestone and sandstone; Triassic strata are scarcely distributed in the middle part, dominated by sandstone. Quaternary sediments are locally exposed, including boulder and sandy gravel. Multi-episode magmatic rocks include the Proterozoic granites in the east and Cenozoic granites in the west [26] (Figure 1b). The structures are dominated by the N-S trending Xianshuihe strike-slip fault that is locally buried by Quaternary sediments [27]. Amounts of NNE-striking secondary fractures are developed along the Xianshuihe fault (Figures 2b, 2c).

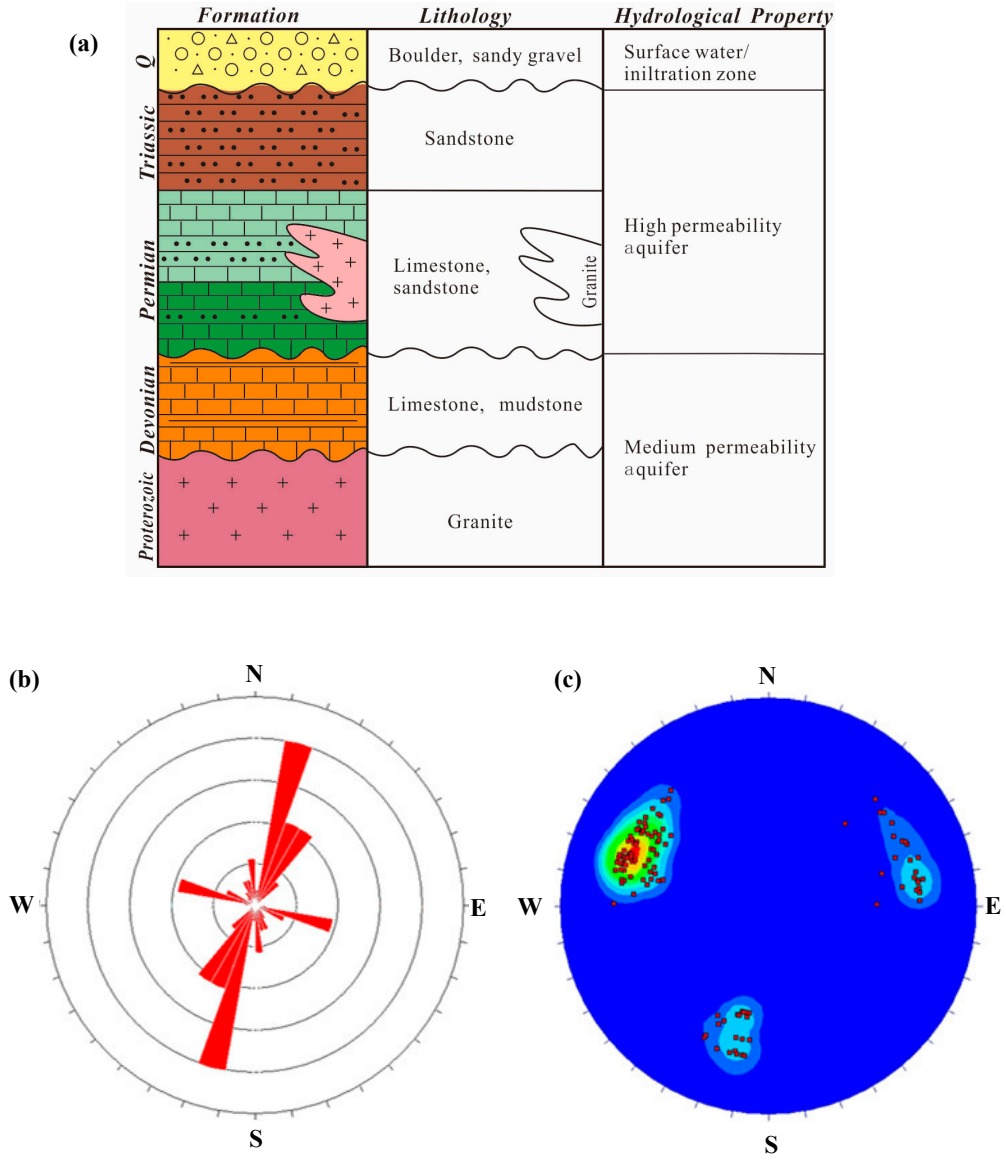

Figure 2. (a) Stratigraphic column showing lithology and hydrological properties, (b) Rose diagram and (c) stereographic diagrams (equal area projection, lower hemisphere) with poles and contouring of fractures in study area. Strata legends are same as Figure 1.

The Dadu River traverses southwardly through Kangding County, fed by a number of streams (Figure 1b). Fractures are extensively distributed in the Triassic sandstone and Cenozoic granite, while karst conduits are developed in the Permian limestone, representing a high permeability aquifer. The less cracked Proterozoic granite and Devonian limestone and mudstone strata represent medium permeability aquifers. Thermal springs are exposed parallel with the Xianshuihe fault, with temperatures over a range of 35°C to 81°C (Local boiling temperature = 89.5 °C) [23-25] (Figures 1b, 1c).

3. Sampling and methods

Sampling work was conducted in November and December, 2012, these months being regarded as the dry season based on local meteorological record. Fifty-three groundwater samples were collected from different cold springs in field crops and fresh rock fractures in tunnels from our study area (Fig. 1b). For comparison, seventy-two surface water samples were collected from the Dadu River and adjacent streams, while fifteen rain samples were collected. Additionally, ten thermal water samples were collected from different thermal springs. 550-ml polyethylene bottles were used to collect water samples. Prior to sampling, these bottles were washed and rinsed at least three times. Hydrochemical analysis of the water samples was performed within ten days in the State Key Laboratory of Geohazard Prevention and Geo-environment Protection, Chengdu University of Technology. HCO_3^- was determined by Gran titration with 0.025 N HCl. Cation samples were preserved with concentrated reagent HCl to pH <1.0. Cations (Na^+, K^+, Ca^{2+}, Mg^{2+}) were analyzed by ICP-OES (ICAP6300) and anions (Cl^-, SO_4^{2-}) by DIONEX (ICS-1100), respectively. Quality measurement for hydrochemical data was tested by ionic balance error (better than ±10 %, calculated by Aquachem 3.7 software). δD and $\delta^{18}O$ isotopes were measured in the Institute of Karst Geology, Chinese Academy of Geological Science, using mass spectrometer (MAT253). The δD and $\delta^{18}O$ analytical precision was better than 1‰ and 0.1‰, respectively.

Phreeqc 3 software is applied to calculate saturation index (SI), based on the MINTEQ database [28]. The SI values of major minerals, containing calcite, dolomite, gypsum, and halite, were calculated to evaluate the chemical equilibrium between minerals and water in nature environment.

Multivariate statistical analysis was carried out using SPSS 20 software. The correlation matrix based on the Pearson's correlation coefficient was used for showing relationships between those variables, with a range of values from -1 to +1. Values close to +1 present strong positive correlation, while values approximate to -1 imply strong negative correlation. Values equal to 0 mean no linear correlation. Principle Component Analysis (PCA) was conducted to analyze the relationship between the variables and evaluate the factors affecting hydrochemical components.

4. Results and discussion

4.1. Hydrochemical characteristics of water samples

Surface water (stream, river), groundwater (fractured water, cold spring), thermal water and rain samples were classified, as shown in Table S1. The Schöeller diagram for those samples is illustrated in Figure 3, indicating the variations of physicochemical parameters.

The surface water and groundwater are neutral to alkaline in nature and have similar chemical compositions, whereas thermal water contains higher concentrations of major ions (Figure 3). The TDS (total dissolved solid) values of surface water, groundwater and thermal water are 52.2-177.1 mg/l, 82.2-227.4 mg/l and 104.6-1666.9 mg/l, respectively. In the most water samples, the anions are dominated by HCO_3^- with abundance order of $HCO_3^- > SO_4^{2-} > Cl^-$, while the main cation is Ca^{2+}, with abundance order of $Ca^{2+} > Na^+ > Mg^{2+} > K^+$. Piper's diagram illustrates the scatter plots of the cations ($Na^+ + K^+$, Ca^{2+}, and Mg^{2+}) and anions (HCO_3^-, Cl^- and SO_4^{2-}), classifying the hydrochemical characteristics [29]. Herein, two main water types have been identified; most water samples were concentrated on the field of Ca^{2+}-HCO_3^-, whereas a few thermal water samples were plotted on the field of Na^+-Cl^- (Figure 4). The greater concentrations of major ions and higher TDS values of thermal water suggest a longer residence time and stronger water-rock interaction.

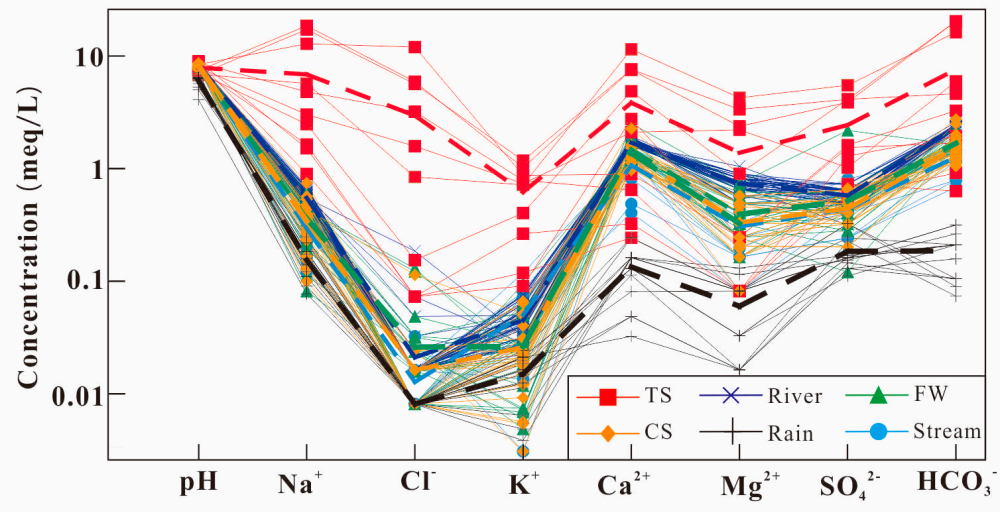

Figure 3. Schöeller diagram for different water samples (unit: meq/l). Dash lines stand for the mean values of different water samples. TS- Thermal spring, CS- Cold spring, FW- Fractured water.

4.2. Hydrochemcial process of surface water and groundwater

4.2.1. Correlation of major ions

The soluble ions of groundwater can be sourced from a variety of natural processes, such as precipitation, evaporation, and water-rock interaction. Gibbs diagram is used to distinguish the effects of these different processes [30]. In the Gibbs TDS versus $Na^+/(Na^+ + Ca^{2+})$ and $Cl^-/(Cl^- + HCO_3^-)$ diagrams, the majority of the samples plotted in the field of rock weathering (Figure 5), indicating water-rock interaction is the main factor controlling dissolved hydrochemical components of water samples.

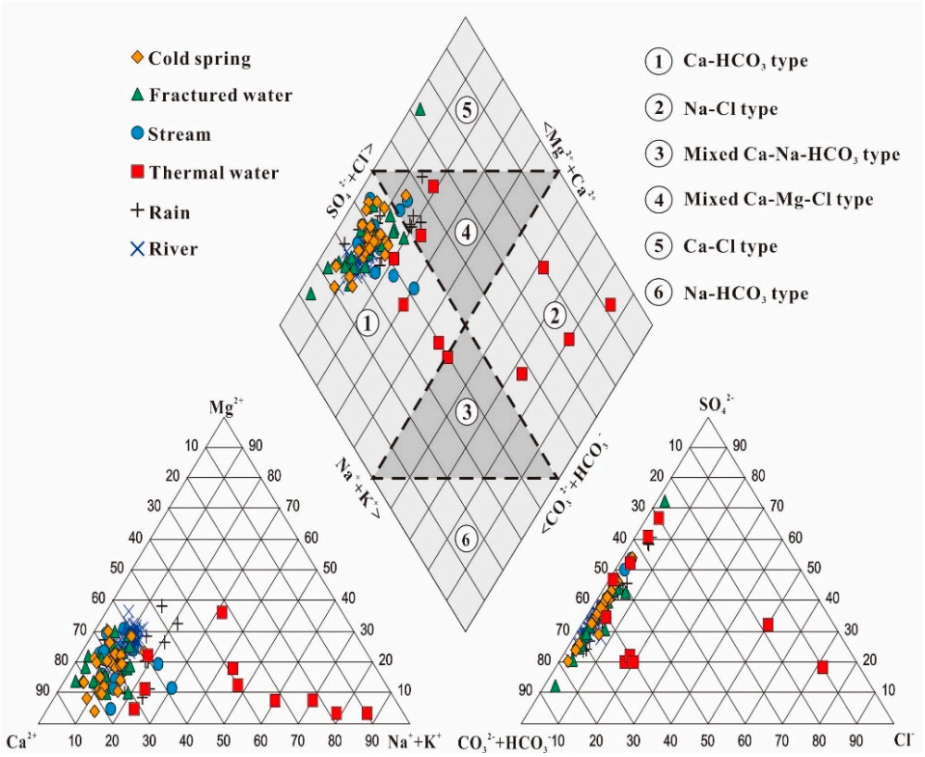

Figure 4. Piper plot of water samples.

Preprints (www.preprints.org) | NOT PEER-REVIEWED | Posted: 17 November 2017 doi:10.20944/preprints201711.0114.v1

Peer-reviewed version available at Water 2018, 10, 80; doi:10.3390/w10010080

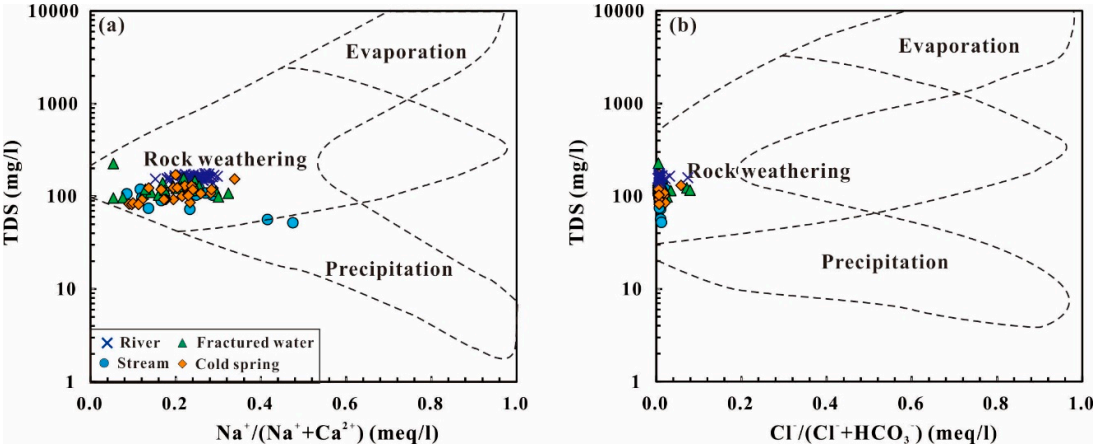

Figure 5. Gibbs plot. (a) TDS versus $Na^+/(Na^+ + Ca^{2+})$, (b) TDS versus $Cl^-/(Cl^- + HCO_3^-)$.

The concentrations of major ions and their correlation give insight to the hydrochemical process triggered by water-rock interaction [31]. Due to the major water type of Ca^{2+}-HCO_3^-, the dissolution of carbonate minerals (calcite and dolomite) should be responsible for the source of Ca^{2+} and HCO_3^- in water, as shown in the following equations (1) and (2).

$$CaCO_3 \text{ (calcite)} + H_2CO_3 \rightarrow Ca^{2+} + 2HCO_3^- \quad (1)$$

$$CaMg(CO_3)_2 \text{ (dolomite)} + 2H_2CO_3 \rightarrow Ca^{2+} + Mg^{2+} + 4HCO_3^- \quad (2)$$

Based on the equations (1) and (2) above, the dissolution of calcite and dolomite would produce the Ca^{2+}/HCO_3^- and $(Ca^{2+} + Mg^{2+})/HCO_3^-$ molar ratio of 0.5. In this study, the Ca^{2+}/HCO_3^- ratios of most samples were between 0.5 and 1 (Figure 6a), while $(Ca^{2+} + Mg^{2+})/HCO_3^-$ ratios were greater than 1 (Figure 6b). Hence, the excess concentrations of Ca^{2+} and Mg^{2+} should be affected by other hydrochemical processes rather than sole dissolution of carbonates (calcite and dolomite). Moreover, the Ca^{2+}/Mg^{2+} molar ratio is used to clarify the dissolution of carbonates [3]. Ca^{2+}/Mg^{2+} molar ratio below 1 triggers dissolution of dolomite, whereas Ca^{2+}/Mg^{2+} molar ratio higher than 1 indicates dissolution of calcite. Additionally, Ca^{2+}/Mg^{2+} molar ratio greater than 2 can be the result of the dissolution of silicate minerals. Most samples had the Ca^{2+}/Mg^{2+} molar ratios largely greater than 2 in this study. Therefore, we can infer Ca^{2+} concentration should be affected by the dissolution of silicate minerals as well.

If Na^+ is derived from the dissolution of halite, the Na^+/Cl^- molar ratio generally is equal to 1. However, the Na^+/Cl^- molar ratio of water samples are much higher than 1, implying the excess Na^+ concentration is derived from silicate weathering (Figure 6c). In addition, the low Cl^- concentration is consistent with the absence of Cl-bearing minerals in Kangding County. The Ca^{2+} and SO_4^{2-} concentrations of groundwater are controlled by gypsum dissolution and precipitation processes, which are shown in equation (3) below.

$$CaSO_4 \cdot 2H_2O \rightleftarrows Ca^{2+} + SO_4^{2-} + 2H_2O \quad (3)$$

In condition of simple gypsum dissolution and precipitation, the ratio between Ca^{2+} and SO_4^{2-} would be 1: 1. The plots are distinctly below 1:1 line in Ca^{2+} versus SO_4^{2-} diagram (Figure 6d), implying a majority of enriched Ca^{2+} that would be produced from dissolution of carbonates and silicate minerals. The deficient SO_4^{2-} concentration suggests weak effect from anthropogenic activity.

The Ca^{2+}, Mg^{2+}, HCO_3^- and SO_4^{2-} would be derived from dissolution of carbonates and sulfate minerals when the plots follow the 1:1 line in the $(Ca^{2+} + Mg^{2+})$ versus $(HCO_3^- + SO_4^{2-})$ diagram. Furthermore, the plots above the 1:1 line suggest ion exchange as dominant process (4), while the plots below the 1:1 line indicate existence of reverse ion exchange (5).

$$\text{Ion exchange: } 2Na^+\text{-Clay} + Ca^{2+} \rightarrow 2Na^+ + Ca^{2+}\text{-Clay}_2 \quad (4)$$

$$\text{Reverse Ion exchange: } Ca^{2+}\text{-Clay}_2 + 2Na^+ \rightarrow Ca^{2+} + 2Na^+\text{-Clay} \quad (5)$$

Most samples plotted above the 1:1 line of (HCO_3^- + SO_4^{2-})/(Ca^{2+} + Mg^{2+}) ratio (Figure 7). The (Ca^{2+} + Mg^{2+}) concentrations are slightly deficient compared with HCO_3^- and SO_4^{2-}. As the dominated cation, Ca^{2+} is more preferable than Mg^{2+}. Considering the equations (4) and (5), we can assume the deficiency of Ca^{2+} is due to ion exchange process that is a significant result from silicate weathering.

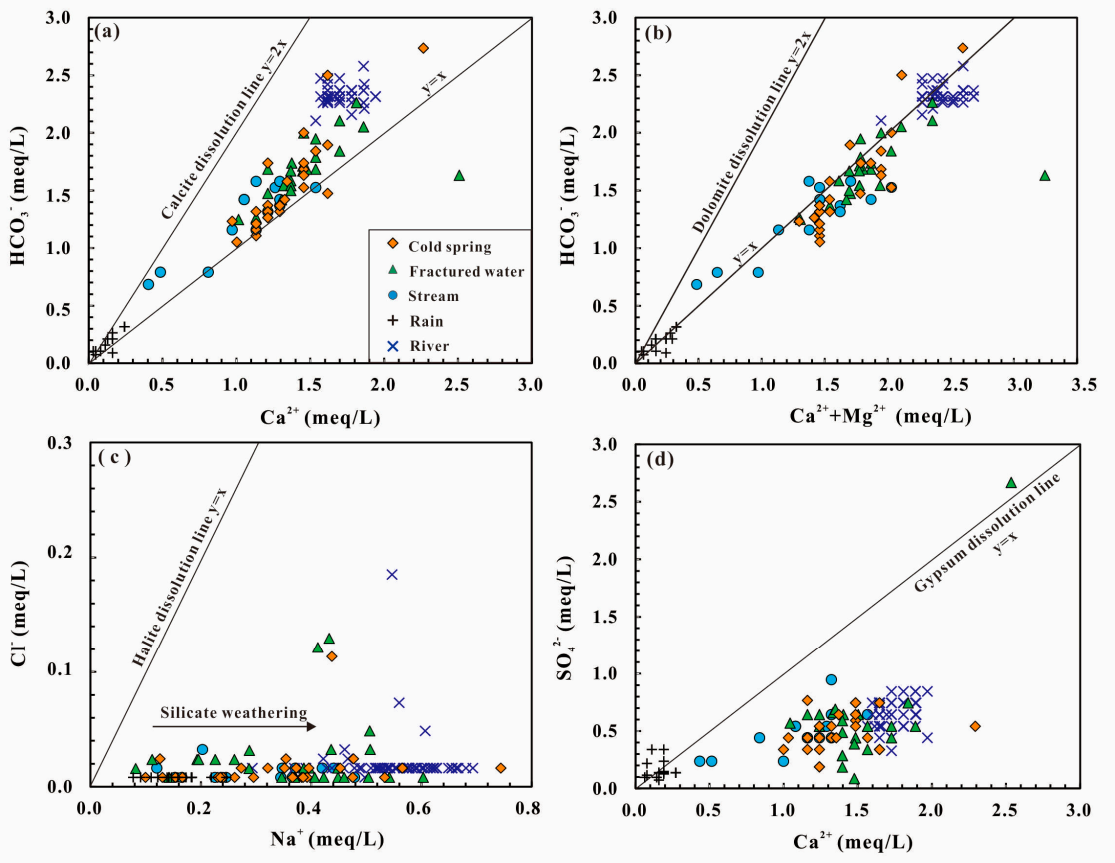

Figure 6. Distributions of ionic ratios in water samples, (a) HCO_3^- versus Ca^{2+}, (b) HCO_3^- versus Ca^{2+} + Mg^{2+}, (c) Cl^- versus Na^+, (d) SO_4^{2-} versus Ca^{2+}.

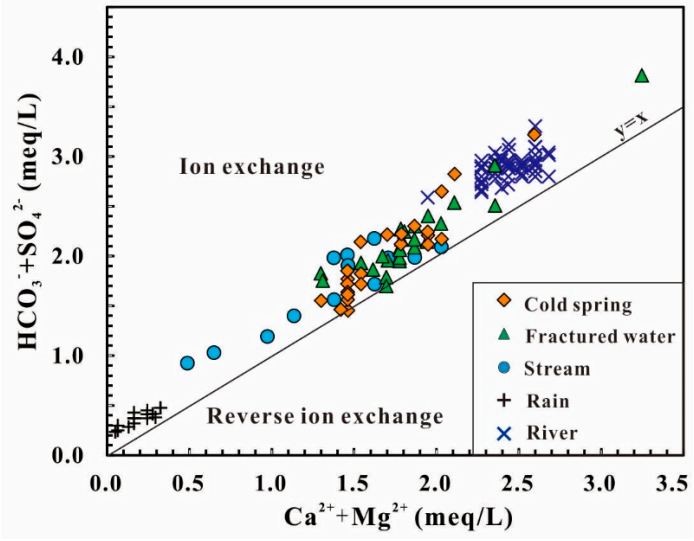

Figure 7. HCO_3^- + SO_4^{2-} versus Ca^{2+} + Mg^{2+} diagram

4.2.2. Mineral saturations

During the process of water-rock interaction, the mineral equilibrium calculation can reflect the thermodynamic process of natural water system [12, 13]. Moreover, Saturation index (SI) gives insight of the reactivity of minerals. Herein, SI values of water samples were calculated using Phreeqc 3 software, based on the equation (6) below,

$$SI = \log (IAP)/K \quad (6)$$

Where IAP is the Ion Activity Product, K is the equilibrium constant. Positive SI values (SI>0) show minerals oversaturation and precipitation, whereas negative SI values (SI<0) imply minerals under saturation and dissolution. The calculated results for surface water and groundwater samples are listed in Table S1. Most water samples yielded similar SI calculated results as follows: calcite and dolomite are slightly under saturated to oversaturated, gypsum is weakly under saturated, and halite is strongly under saturated (Figure 8). Those calculated results propose water-rock interaction has not reached to equilibrium yet in surface water and groundwater of Kangding County. In equation (3), abundant Ca^{2+} released from the dissolution of calcite will hamper the solubility of $CaSO_4 \cdot 2H_2O$, leading to the under saturation of gypsum. The absence of Cl^--bearing minerals would account for the low SI values of halite. Due to the positive correlation between SI values and TDS, the hydrochemical characteristics of surface water and groundwater are mainly determined by the dissolution and precipitation of minerals from bedrocks.

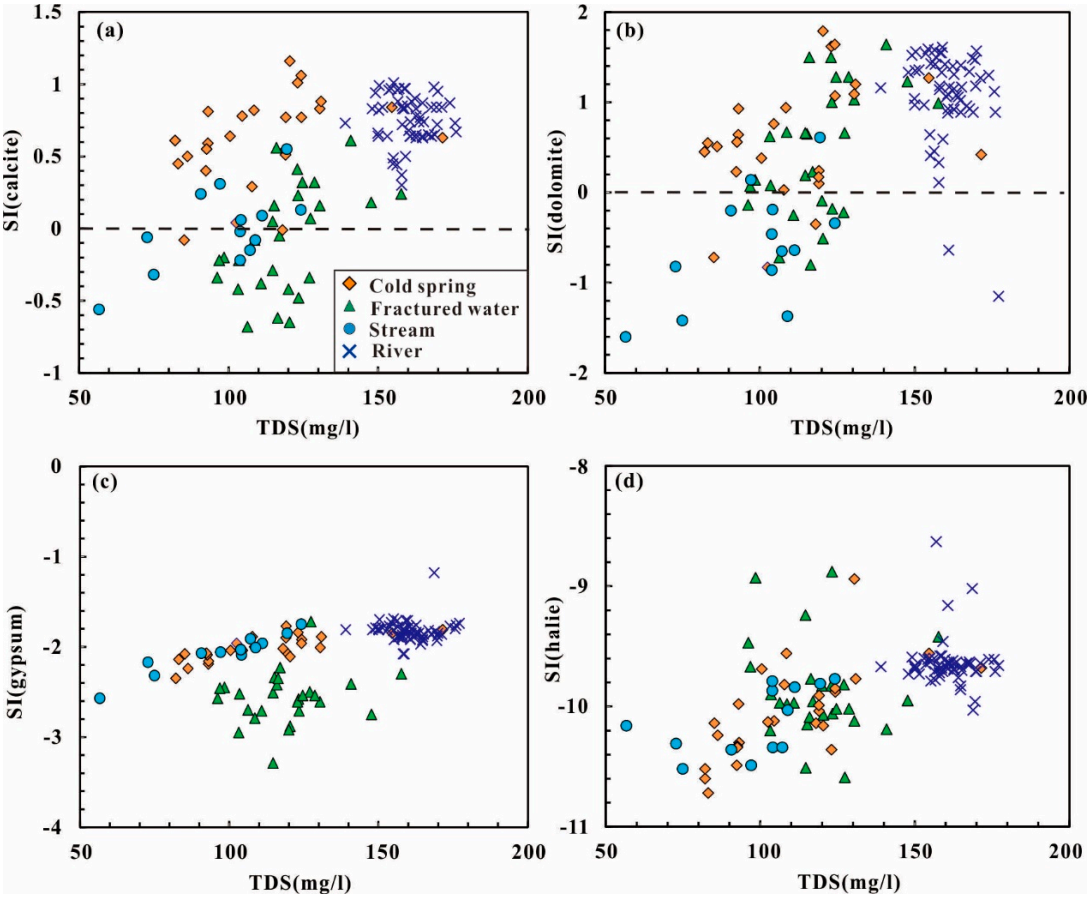

Figure 8. SI (calcite), SI (dolomite), SI (gypsum), and SI (halite) values versus TDS (mg/l) diagrams

4.2.3. Multivariate statistical analysis

The correlations applied to the eight variables (pH and major ions) shed light on the relationships among those variables and water-rock interaction controlling the hydrochemical parameters. The values of R>0.75 and 0.75>R>0.50 suggest strong and moderate correlations between the hydrochemical parameters, respectively. The results of correlation analysis are listed in Table 1. Ca^{2+} shows great consistency with Mg^{2+}, representing the aquifer system of carbonates. pH has moderate and negative correlation with carbonates elements (Ca^{2+}, Mg^{2+} and HCO_3^-), indicating the chemical equilibrium between pH and dissolution of carbonates. However, the correlation between Ca^{2+}, Mg^{2+} and HCO_3^- are not as high as expected, inconsistent with simple source from the dissolution of carbonates. In addition, the negative correlation between Ca^{2+}, Mg^{2+} and Na^+ reveals the possibility of ion exchange process from the dissolution of silicate minerals. The pairs of Ca^{2+}-SO_4^{2-} and Na^+-Cl^- have weak correlation, respectively, suggesting they are not considerably affected by the simple dissolution of gypsum or halite.

Table 1. Correlation matrix of the species in water samples.

Correlation	pH	Na^+	Cl^-	K^+	Ca^{2+}	Mg^{2+}	SO_4^{2-}	HCO_3^-
pH	1.000							
Na^+	0.535	1.000						
Cl^-	0.251	0.424	1.000					
K^+	0.360	0.691	0.483	1.000				
Ca^{2+}	-0.378	-0.422	-0.138	0.074	1.000			
Mg^{2+}	-0.225	-0.351	-0.110	0.094	0.755	1.000		
SO_4^{2-}	0.424	0.373	0.040	0.201	0.426	0.479	1.000	
HCO_3^-	-0.374	0.494	-0.077	0.213	0.436	0.349	0.515	1.000

Table 2. Factor loadings and eigenvalues of the eight extracted factors.

Scaled Coordinates	PC1	PC2
pH	0.808	-0.119
Na^+	0.679	-0.601
Cl^-	0.166	-0.832
K^+	0.427	-0.738
Ca^{2+}	0.872	0.388
Mg^{2+}	0.819	0.350
SO_4^{2-}	0.405	0.129
HCO_3^-	0.917	0.264
Eigenvalues	4.090	1.971
%Variance	51.120	24.640
Cumulative %	51.120	75.760

Hydrochemical parameters including pH and major ions were used for principal component analysis, which is helpful to trace the sources of those ions. The results of principal component analysis includes eigenvalue, percentage of variance, cumulative percentage of variance, and the factor loading, presented in Table 2. Scree plot for groundwater samples showed a distinct change of slop after the third factor (Figure 9a). Using the Kaiser Criterion and scree plot, two major factors of eigenvalues greater than 1 have been obtained, accounting for the total variance of 75.76% (Figure 9b). The dominant factor (PC1) is responsible for 51.12 % of total variance and has a strong loading of pH, Na^+ Ca^{2+}, Mg^{2+}, and HCO_3^-. This factor indicates the general trend of hydrochemcial characteristics and is probably dominated by the dissolution of carbonates and silicate minerals with ion exchange process. The second factor (PC2) explains 24.64 % of total variance and has medium

positive loading of Ca^{2+}, Mg^{2+} and SO_4^{2-}. Due to the dissolution of carbonates, amounts of Ca^{2+} are occurred in water, restraining the dissolution of gypsum. As such, PC2 could be linked to weak dissolution of gypsum. In addition, the negative loading of Na^+ and Cl^- is exhibited, indicating Na^+ and Cl^- concentrations are determined by different factors rather than simple dissolution of halite.

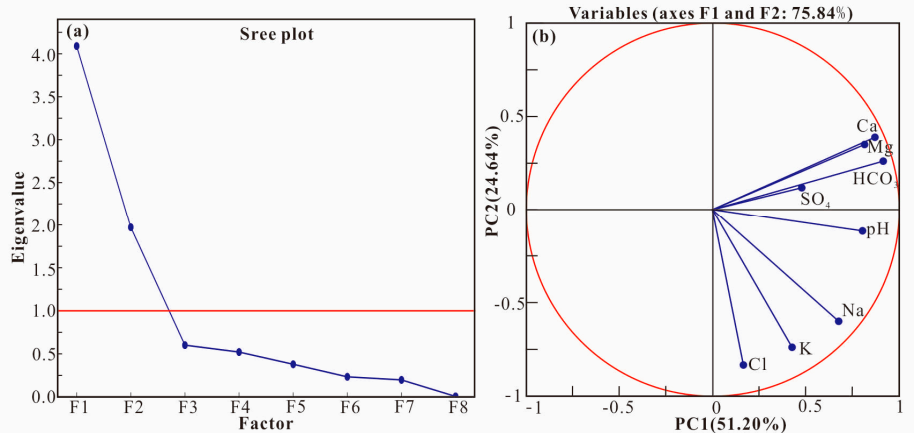

Figure 9. (a) Scree plot, (b) Factor loadings for the PC1 and PC2.

4.3. Mixing model of groundwater and thermal water

The main anions (Cl^-, SO_4^{2-} and HCO_3^-) have been used to identify the mixture between thermal and cold water [32]. The majority of thermal water samples are distributed on the field of peripheral water (Figure 10a), indicative of the involvement of cold water. Furthermore, the Na-K-Mg ternary diagram shows that all thermal water samples are typical of immature water [32] (Figure 10b), as well as relatively deficient saturated indices of different minerals in Table S1. Giggenbach and Goguel (1989) suggested the low equilibrium of thermal water would be attributed to the dilution and mixing of surficial cold water [33]. The water-rock equilibrium at different temperatures is interpreted using the $10Mg^{2+}/(10Mg^{2+} + Ca^{2+})$ versus $10K^+/(10K^+ + Na^+)$ diagram. In Figure 10c, all thermal water samples plotted above the curved line of the full equilibrium, yielding the recharge of cold water. Hence, we can infer that thermal water is typical of immature water, involved with cold water.

To evaluate the original temperature of thermal water and mixing ratio of cold water, the field temperatures and silica concentration of thermal and cold water have been extensively carried out [34, 35], based on the equations (7) and (8) below:

$$S_c x + S_h (1-x) = S_s \quad (7)$$

$$SiO_{2c} + SiO_{2h} (1-x) = SiO_{2s} \quad (8)$$

Where S_c is enthalpy of cold water, S_h is the initial enthalpy of deep thermal water, S_s is the last enthalpy of thermal water, SiO_{2c} is SiO_2 concentration of cold water, SiO_{2h} is the beginning SiO_2 content of deep thermal water, SiO_{2s} is SiO_2 concentration of thermal water. Founier and Truesdell (1974) proposed a graphical way to obtain the two unknowns [34]. In the Figure 11, red and blue curves are drawn, and their intersections represent the mixing portion of cold water and estimated reservoir temperature. Based on the results from Fig. 11, we can infer the original temperature and mixing ratio are 112-195 °C and 0.56-0.79, respectively. Moreover, a silicon-enthalpy graphic method has been conducted to estimate the reservoir temperature of mixing water [33]. It is assumed no silica deposition existed before or after mixing and that quartz determines the solubility of silica in thermal water. A straight line connecting point of cold water and points of thermal water intersects with the solubility curve for quartz at a point that gives the silica content and enthalpy value of thermal water in the condition of no steam loss (Figure 10d). If steam separation took place at 89.5 °C (local boiling temperature), the calculated reservoir temperature is 148 °C. When no steam loss occurs, the reservoir temperatures range from 130 °C to 199 °C, consistent with the calculated results

Preprints (www.preprints.org) | NOT PEER-REVIEWED | Posted: 17 November 2017 doi:10.20944/preprints201711.0114.v1

Peer-reviewed version available at Water 2018, 10, 80; doi:10.3390/w10010080

from mixing ratio model. Hence, the calculated temperatures should be reliable. It is noteworthy that the estimated reservoir temperatures are much greater than the discharge temperature, suggesting plenty of cold-water recharge in surficial place.

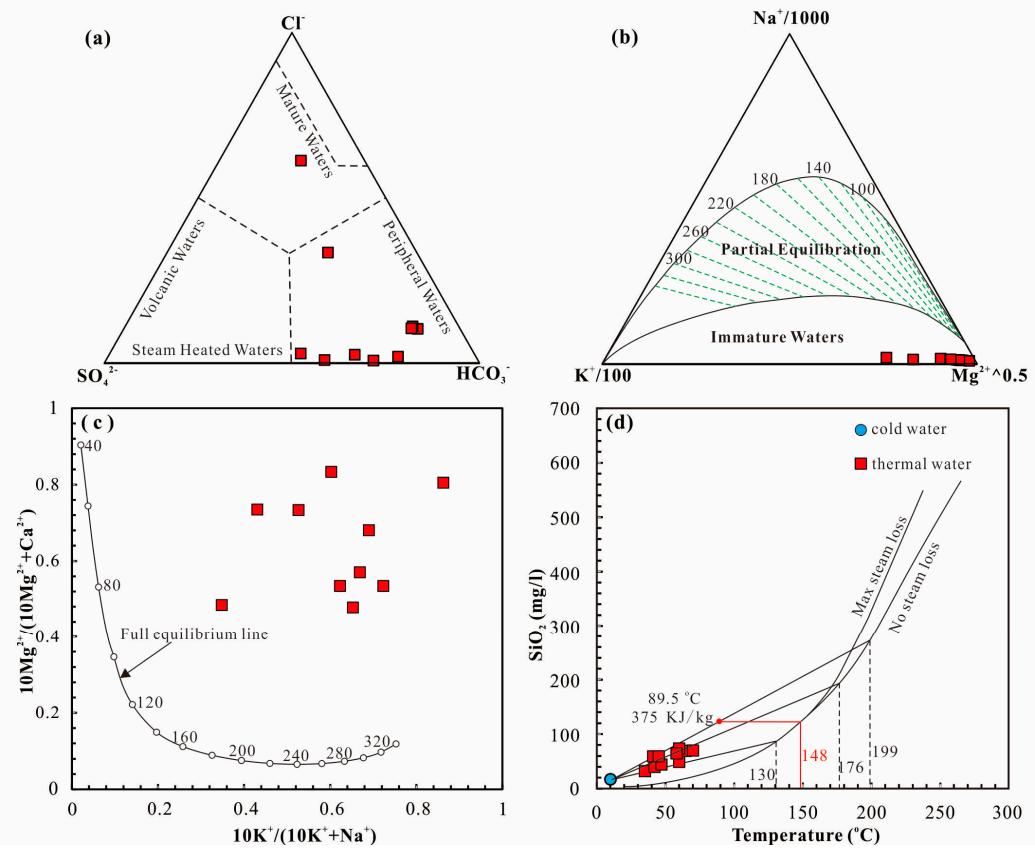

Figure 10. (a) Giggenbach Cl^--SO_4^{2-}-HCO_3^- and (b) Na-K-Mg ternary diagrams, (c) $Mg^{2+}/(Mg^{2+} + Ca^{2+})$ versus $10K^+/(10K^+ + Na^+)$ diagram, (d) SiO_2 versus temperature diagram. Silica concentration of cold water is the average values of groundwater samples in Table S1.

4.4. Evaluation for δD and $\delta^{18}O$ isotopes

The results of δD and $\delta^{18}O$ isotopes from surface water (river), groundwater (cold spring and fractured water) and thermal water were list in Table S2. The δD and $\delta^{18}O$ values of surface water and groundwater in study area have a similar range of -75.39 to -86.47‰ and -11.01 to -12.47‰, while δD and $\delta^{18}O$ values of thermal water largely vary from -78.77 to -113.27 ‰ and -10.04 to -16.13‰, respectively. Compared to thermal water, surface water and groundwater have richer δD values. Most samples were distributed around the Global Meteoric Water Line (GMWL) (solid line: $\delta D = 8*\delta^{18}O + 10‰$) [36] and Local Meteoric Water Line (LMWL) (dash line: $\delta D = 9.4*\delta^{18}O + 28.5‰$) [37], indicating a meteoric origin (Figure 12). It is generally acceptable that δD and $\delta^{18}O$ values will decrease corresponding to changing elevation, due to topographic precipitation [38]. Hence, using the recharge altitude calculated by δD and $\delta^{18}O$ values, we can constrain the general recharge area of those water samples. In study area, the ratio between δD and altitude has been suggested in -2.24‰ per 100 m [37]. The calculated results present the recharge altitudes of surface water and groundwater are 1059-1517 m. The recharge area of thermal water is located in a large variation of 2199-5302 m, greatly higher than those of surface water and groundwater. Therefore, we can propose thermal water is recharged by precipitation from high elevation, while surface water and groundwater are recharged by precipitation from low elevation. Moreover, obvious $\delta^{18}O$ drift in Figure 12 suggests thermal water experienced remarkable and prolonged water-rock interaction during the deep circulation, corresponding to high TDS and concentrations of major ions.

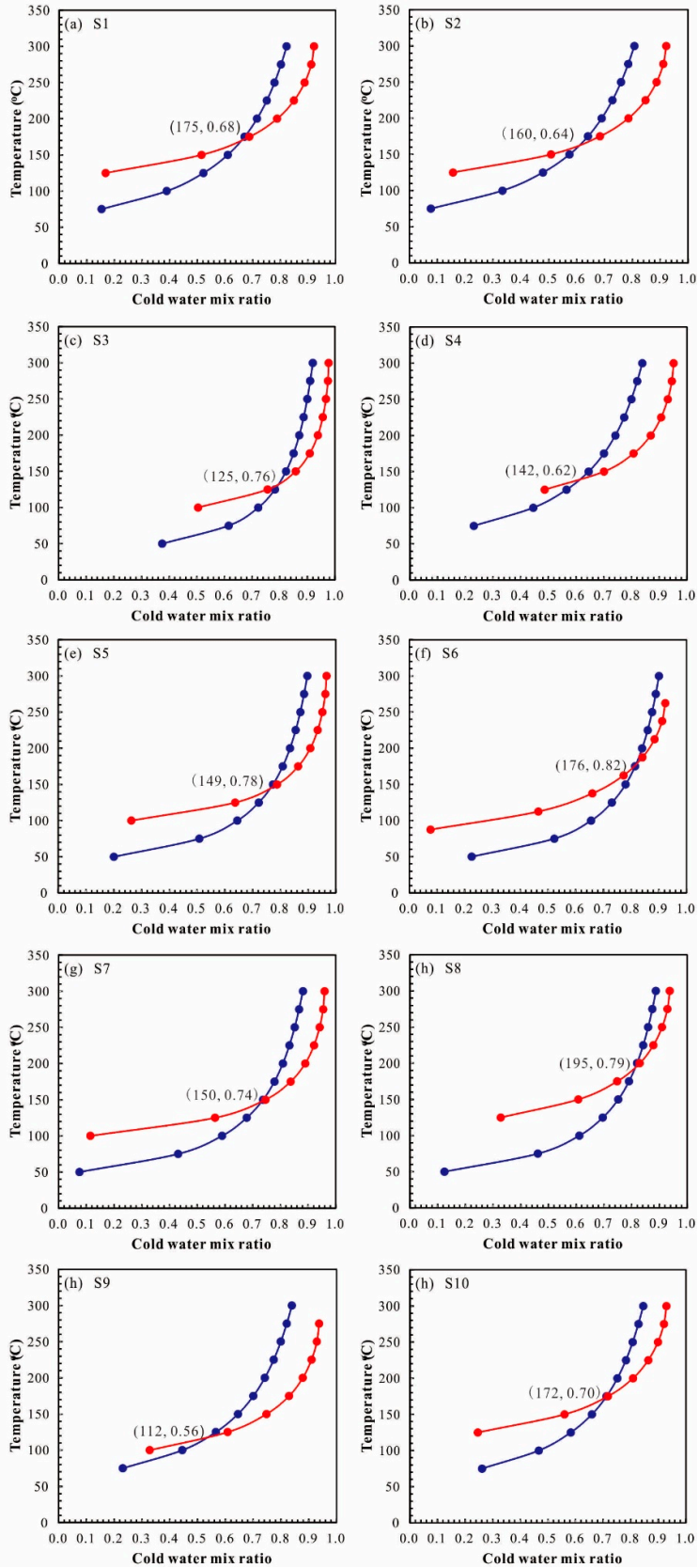

Figure 11. Relations between fraction of cold water and temperature in the mixing model. Blue curve = enthalpy, red curve = silica.

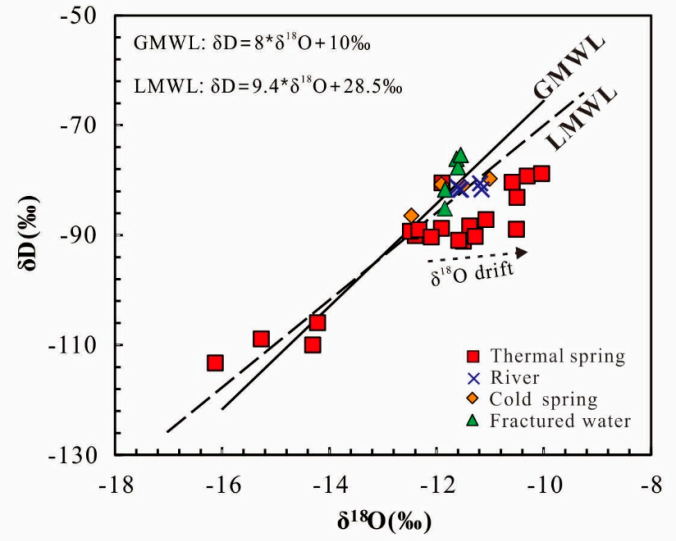

Figure 12. Variation of δD and $\delta^{18}O$ in groundwater and thermal springs associated with Global Meteoric Water Line (GMWL) [36] and Local Meteoric Water Line (LMWL) [37].

4.5. Hydrological conceptual model of natural water system

Based on the aforementioned geological setting, hydrochemical and isotopic analyses above, a hydrological conceptual model for the natural water system (surface water, groundwater, and thermal water) in Kangding County has been constructed (Figure 13). A joint study of the ratio of major ions, geochemical modelling, and multivariate statistical analysis concluded hydrochemical processes of surface water and groundwater are dominated by the dissolution of carbonates and silicate minerals, corresponding to the limestone and granite aquifers in Kangding County. δD and $\delta^{18}O$ isotopic results show the high recharge elevations of 2199-5302 m, implying the potential recharge area from the Mount. Gongga (7556 m) and adjacent mountain areas. Based on the concentrations of major ions and SiO_2, thermal water samples have been identified as immature water, within cold-water mixing ratio of 0.56-0.79. Meanwhile, the discharge temperatures in surficial place are much lower than the estimated reservoir temperatures, indicative of large involvement of cold water. The N-S direction Xianshuihe fault and adjacent NNE-striking secondary fractures are responsible for vertical and lateral flow in natural water system. Herein, it is reasonable that abundant groundwater penetrating through those fractures recharges the thermal aquifer system. Additionally, the favorable hydraulic connection between surface water and groundwater has been determined by their similar hydrochemical and δD-$\delta^{18}O$ isotopic characteristics. Therefore, we can conclud the Xianshuihe fault provides the deep channel for upwelling of thermal water, while those fractures are the ideal chamber for the surface water-groundwater interaction and recharge to thermal water in surficial place.

5. Conclusion

Integrated assessments of variable data based on hydrochemical analysis, multivariate statistics and geochemical modelling, provide the basis for comprehensive understanding of natural water system in Kangding County, which can be summarized as follows:

(1) Surface water and groundwater are dominated by Ca-HCO_3 type, while thermal water belongs to Ca-HCO_3 and Na-Cl type.

(2) Correlations of major ions, multivariate statistical analysis, and saturation index indicated the dissolution of carbonates and silicate minerals were the main hydrochemical processes affecting chemical components of natural water system in limestone and granite aquifers. Detailed effects of

anthropogenic activity on hydrochemistry have yet to be further investigated yet by more minor elements in future.

(3) Thermal water is typical of immature water that is involved with cold-water fraction of 0.56-0.79. The estimated reservoir temperatures have a range of 130 °C to 199 °C.

(4) δD and $\delta^{18}O$ isotopes revealed a meteoric origin of hydrological system. Thermal water is recharged by precipitation from high elevation, while surface water and groundwater are recharged by precipitation from low elevation.

(5) The Xianshuihe fault is the rising channel for thermal water, while adjacent secondary fractures provide the chambers for groundwater-surface water interaction and groundwater recharging with thermal water.

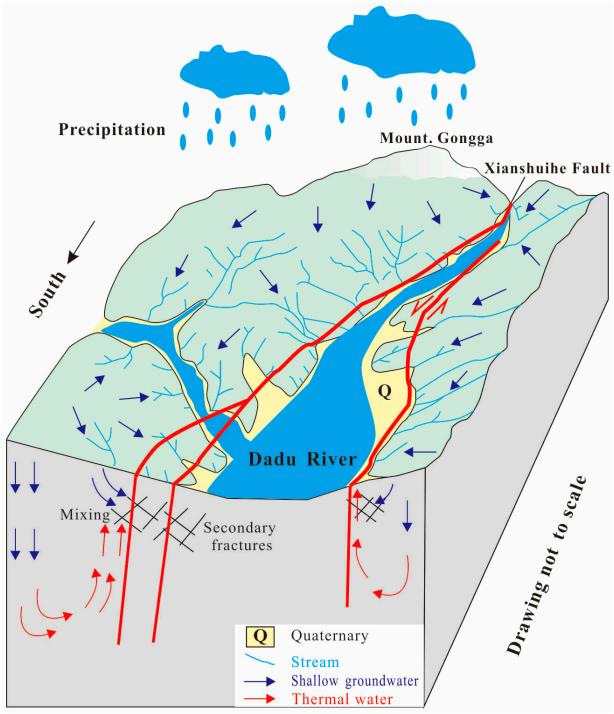

Figure 13. Hydrological conceptual model of natural water system in Kangding County

Supplementary Materials: The following are available online at www.mdpi.com/link, Table S1: Hydrochemical composition of water samples, Table S2: δD and $\delta^{18}O$ isotopes of representative water samples.

Acknowledgments: We thank anonymous reviewers and the Editor-in-Chief for their constructive comments. We thank Prof. Jing Yu and Ziwen Hu at the State Key Laboratory of Geohazard Prevention and Geo-environment Protection, Chengdu University of Technology for their assistance and helpful discussions. We also be grateful to the English editing by Mr. Conor O'Sullivan.

Author Contributions: Yunhui Zhang, Mo Xu and Xiao Li conceived and designed the research direction. Yunhui Zhang wrote the paper. Jihong Qi, Qiang Zhang and Leilei Yu did the field work and collected water samples; Jian Guo and Rui Zhao performed the experiments and analyzed the data. All authors read and approved the final manuscript.

Conflicts of Interest: The authors declare no conflict of interest.

References

1. Rakotondrabe, F.; Ngoupayou, J.R.N.; Mfonka, Z.; Rasolomanana, E.H.; Abolo, A.J.N.; Ako, A.A. Water quality assessment in the Betare-Oya gold mining area (East-Cameroon): Multivariate Statistical Analysis approach. *Sci Total Environ*. **2018**, 610-611, 831-844. doi.org/10.1016/j.scitotenv.2017.08.080

2. Kazakis, N.; Matta, C.; Pavlou, A.; Patrikaki, O.; Voudouris, K. Multivariate statistical analysis for the assessment of groundwater quality under different hydrogeological regimes. *Environmental Earth Sciences*. **2017**, 76, 349-361. doi.org/10.1007/s12665-017-6665-y
3. Hamzah, Z.; Aris, A.Z.; Ramli, M.F.; Juahir, H.; Narany, T.S. Groundwater quality assessment using integrated geochemical methods, multivariate statistical analysis, and geostatistical technique in shallow coastal aquifer of Terengganu, Malaysia. *Arabian Journal of Geosciences*. **2017**, 10, 49-65. doi.org/10.1007/s12517-016-2828-5
4. Xiao, Y.; Gu, X.M.; Yin, S.Y.; Pan, X.Y.; Shao, J.L.; Cui, Y.L. Investigation of Geochemical Characteristics and Controlling Processes of Groundwater in a Typical Long-Term Reclaimed Water Use Area. *Water*. **2017**, 9, 800-815. doi:10.3390/w9100800
5. Gu, X.M.; Zhang, Q.L.; Cui, Y.L.; Shao, J.L.; Xiao, Y.; Zhang, P.; Liu, J.X. Hydrogeochemistry and Genesis Analysis of Thermal and Mineral Springs in Arxan, Northeastern China. *Water*. **2017**, 9, 61-77. doi:10.3390/w9010061
6. Wu, X.; Zheng, Y.; Zhang, J.; Wu, B.; Wang, S.; Tian, Y.; Li, J.G.; Meng, X. Investigating Hydrochemical Groundwater Processes in an Inland Agricultural Area with Limited Data: A Clustering Approach. *Water*. **2017**, 9, 723-742. doi:10.3390/w9090723
7. Pasvanoğlu, S.; Çelik, M. A conceptual model for groundwater flow and geochemical evolution of thermal fluids at the Kızılcahamam geothermal area, Galatian volcanic Province. *Geothermics*. **2018**, 71, 88-107. doi.org/10.1016/j.geothermics.2017.08.012
8. Yurteri, C.; Simsek, S. Hydrogeological and hydrochemical studies of the Kaman-Savcili-Büyükoba (Kirsehir) geothermal area, Turkey. *Geothermics*. **2017**. 65, 99-112. doi.org/10.1016/j.geothermics.2016.09.002
9. Yang, P.H.; Cheng, Q.; Xie, S.Y.; Wang, J.L.; Chang, L.R.; Yu, Q.; Zhan, Z.J.; Chen, F. Hydrogeochemistry and geothermometry of deep thermal water in the carbonate formation in the main urban area of Chongqing, China. *Journal of Hydrology*. **2017**, 549, 50-61. doi.org/10.1016/j.jhydrol.2017.03.054
10. Wang, X.C.; Zhou, X.; Zheng, Y.H.; Song, C.; Long, M.; Chen, T.; Ren, Z.H.; Yang, M.L.; Li, X.L.; Guo, J. Hydrochemical characteristics and mixing behavior of thermal springs along the Bijiang River in the Lanping basin of China. *Environmental Earth Sciences*. **2017**, 76, 487-505. doi.org/10.1007/s12665-017-6821-4
11. Tziritis, E.P.; Datta, P.S.; Barzegar, R. Characterization and Assessment of Groundwater Resources in a Complex Hydrological Basin of Central Greece (Kopaida basin) with the Joint Use of Hydrogeochemical Analysis, Multivariate Statistics and Stable Isotopes. *Aquatic Geochemistry*. **2017**, 23, 271-298. doi.org/10.1007/s10498-017-9322-x
12. Singh, C.K.; Kumar, A.; Shashtri, S.; Kumar, A.; Kumar, P.; Mallick, J. Multivariate statistical analysis and geochemical modeling for geochemical assessment of groundwater of Delhi, India. *Journal of Geochemical Exploration*. **2017**, 175, 59-71. doi.org/10.1016/j.gexplo.2017.01.001
13. Liu, P.; Hoth, N.; Drebenstedt, C.; Sun, Y.J.; Xi, Z.M. Hydro-geochemical paths of multi-layer groundwater system in coal mining regions-Using multivariate statistics and geochemical modeling approaches. *Sci of Total Environ*. **2017**, 601-602, 1-14. doi.org/10.1016/j.scitotenv.2017.05.146
14. Gil-Márquez, J.M.; Barberá, J.A.; Mudarra, B.A.M. Hydrological and geochemical processes constraining groundwater salinity in wetland areas related to evaporitic (karst) systems. A case study from Southern Spain. *Journal of Hydrology*. **2017**, 544, 538-554. doi.org/10.1016/j.jhydrol.2016.11.062
15. Wu, J.H.; Li, P.Y.; Qian, H.; Duan, Z.; Zhang, X.D. Using correlation and multivariate statistical analysis to identify hydrogeochemical processes affecting the major ion chemistry of waters: a case study in Laoheba phosphorite mine in Sichuan, China. *Arabian Journal of Geosciences*. **2013**, 7, 3973-3982. doi.org/10.1007/s12517-013-1057-4
16. Kumar, M.S.; Dhakate, R.; Yadagiri, G.; Reddy, K,S. Principal component and multivariate statistical approach for evaluation of hydrochemical characterization of fluoride-rich groundwater of Shaslar Vagu watershed, Nalgonda District, India. *Arabian Journal of Geosciences*. **2017**, 10, 83-99. doi.org/10.1007/s12517-017-2863-x
17. Argamasilla, M.; Barbera, J.A.; Andreo, B. Factors controlling groundwater salinization and hydrogeochemical processes in coastal aquifers from southern Spain. *Sci of Total Environ*. **2017**, 580, 50-68. doi.org/10.1016/j.scitotenv.2016.11.173

18. Yuan, J.F.; Xu, F.; Deng, G.S.; Tang, Y.Q. Using stable isotopes and major ions to identify hydrogeochemical characteristics of karst groundwater in Xide country, Sichuan Province. *Carbonates and Evaporites. 2017*, online, 1-12. doi.org/10.1007/s13146-017-0333-x
19. Papp, D.C., Cociuba, I.; Baciu, C.; Cozma, A. Origin and Geochemistry of Mine Water and its Impact on the Groundwater and Surface Running Water in Post-mining Environments: Zlatna Gold Mining Area (Romania). *Aquatic Geochemistry*. **2017**, 23, 247-270. doi.org/10.1007/s10498-017-9321-y
20. Wang, S.Q.; Liu, Z.; Shao, J.L. Hydrochemistry and H-O-C-S Isotopic Geochemistry Characteristics of Geothermal Water in Nyemo-Nagqu, Tibet. *Acta Geologica Sinica (English Edition)*. **2017**, 91, 644-657. doi: 10.1111/1755-6724.13123
21. Tiwari, S.K.; Rai, S.K.; Bartarya, S.K.; Gupta, A.K.; Negi, M. Stable isotopes ($\delta^{13}C_{DIC}$, δD, $\delta^{18}O$) and geochemical characteristics of geothermal springs of Ladakh and Himachal (India): Evidence for CO_2 discharge in northwest Himalaya. *Geothermics*. **2016**, 64, 314-330. doi.org/10.1016/j.geothermics.2016.06.012
22. Sun, Z.; Ma, R.; Wang, Y.X.; Hu, Y.L.; Sun, L.J. Hydrogeological and hydrogeochemical control of groundwater salinity in an arid inland basin: Dunhuang Basin, northwestern China. *Hydrological Processes*. **2016**, 30, 1884-1902. doi: 10.1002/hyp.10760
23. Qi, J.H.; Xu, M.; An, C.J.; Wu, M.L.; Zhang, Y.H.; Li, Xiao.; Zhang, Q.; Lu, G.P. Characterizations of geothermal springs along the Moxi deep fault in the western Sichuan plateau, China. *Physics of the Earth and Planetary Interiors*. **2017**, 263, 12-22. doi.org/10.1016/j.pepi.2017.01.001
24. Luo, J.; Pang, Z.H.; Kong, Y.K.; Wang, Y.C. Geothermal potential evaluation and development prioritization based on geochemistry of geothermal waters from Kangding area, western Sichuan, China. *Environmental Earth Sciences*. **2017**, 76, 343-366. doi.org/10.1007/s12665-017-6659-9
25. Guo, Q.; Pang, Z.H.; Wang, Y.C.; Tian, J. Fluid geochemistry and geothermometry applications of the Kangding high-temperature geothermal system in eastern Himalayas. *Applied Geochemistry*. **2017**, 81, 63-75. doi.org/10.1016/j.apgeochem.2017.03.007
26. Zhang, Y.Z.; Replumaz, A.; Leloup, P.H.; Wang, G.C.; Bernet, M.; Beek, P.; Paquette, J.L.; Chevalier, M.L. Cooling history of the Gongga batholith: Implications for the Xianshuihe Fault and Miocene kinematics of SE Tibet. *Earth and Planetary Science Letters*. **2017**, 465, 1-15. doi.org/10.1016/j.epsl.2017.02.025
27. Yan, B.; Lin, A.M. Holocene activity and paleoseismicity of the Selaha Fault, southeastern segment of the strike-slip Xianshuihe Fault Zone, Tibetan Plateau. *Tectonophysics*. **2017**, 694, 302-318. doi.org/10.1016/j.tecto.2016.11.014
28. Parkhurst, D.L., Appelo, C.A.J. Description of input and examples for PHREEQC version 3: a computer program for speciation, batch-reaction, one-dimensional transport, and inverse geochemical calculations. *Groundwater in Book 6 Modeling Techniques*. **2013**, US Geological Survey, 6-A43. https://pubs.er.usgs.gov/publication/tm6A43
29. Piper, A.M. A graphic procedure in the geochemical interpretation of water-analyses. *Eos, Transactions American Geophysical Union*. **1944**, 25, 914-928. doi:10.1029/TR025i006p00914
30. Gibbs, R.J. Mechanisms controlling world water chemistry. *Science*. **1970**, 170, 1088-1090. doi:10.1126/science.170.3962.1088
31. Adams, S.; Titus, R.; Pietersen, K.; Tredoux, G.; Harris, C. Hydrochemical characteristics of aquifers near Sutherland in the Western Karoo, South Africa. *Journal of Hydrology*. **2001**, 241, 91-103. doi.org/10.1016/S0022-1694(00)00370-X
32. Giggenbach, W.F. Geothermal solute equilibria. Derivation of Na-K-Mg-Ca geoindicators. *Geochimica et cosmochimica acta*. **1988**, 52, 2749-2765. doi.org/10.1016/0016-7037(88)90143-3
33. Giggenbach, W.F.; Goguel R.L. Collection and analysis of geothermal and volcanic water and gas discharges. *DSIR report CD 2401, 4th ed. Pentone, New Zealand*. **1989**, 81. https://openei.org/wiki/Collection_and_Analysis_of_Geothermal_and_Volcanic_Water_and_Gas_Discharges
34. Fournier R.O. Geochemical indicators of subsurface temperature-part 2, estimation of temperature and fraction of hot water mixed with cold. *Jour. Research US Geol. Survey*. **1974**, 2, 263-270. https://pubs.er.usgs.gov/publication/ofr741032
35. Gupta, H.K.; Roy, S. Geothermal energy: an alternative resource for the 21st century. *2006*, Elsevier. 74-77.https://books.google.ie/books?hl=en&lr=&id=3sOyhcp5eZYC&oi=fnd&pg=PP1&dq=Geothermal+energy:+an+alternative+resource+for+the+21st+century&ots=AogjZfXQkX&sig=0mistkcZUw5urYAG1uc

LjfaeqJw&redir_esc=y#v=onepage&q=Geothermal%20energy%3A%20an%20alternative%20resource%20for%20the%2021st%20century&f=false

36. Craig, H. Isotopic variations in meteoric waters. *Science*. **1961**, 133, 1702-1703. http://links.jstor.org/sici?sici=0036-8075%2819610526%293%3A133%3A3465%3C1702%3AIVIMW%3E2.0.C0%3B2-J

37. Song, C.L, Sun, X.Y., Wang, G.X. (2015). A study on precipitation stable isotopes characteristics and vapor sources of the subalpine Gongga Mountain, China. *Resources and Environment in the Yangtze basin*. **24**, 1860-1869. (In Chinese and English abstract) doi:10.11870/cjlyzyyhj201511008

38. Blasch, K.W.; Bryson, J.R. Distinguishing sources of ground water recharge by using δ^2H and $\delta^{18}O$. *Groundwater*. **2007**, 45, 294-308. doi:10.1111/j.1745-6584.2006.00289.x